Inorganic Chemistry

Article

pubs.acs.org/IC

Hydrothermal Synthesis and Characterization of Novel Brackebuschite-Type Transition Metal Vanadates: $Ba_2M(VO_4)_2(OH)$, M = V^{3+}, Mn^{3+}, and Fe^{3+}, with Interesting Jahn–Teller and Spin-Liquid Behavior

Liurukara D. Sanjeewa,[†] Michael A. McGuire,[‡] Vasile O. Garlea,[§] Longyu Hu,[†] George Chumanov,[†] Colin D. McMillen,[†] and Joseph W. Kolis*,[†]

[†]Department of Chemistry and Center for Optical Materials Science and Engineering Technologies (COMSET), Clemson University, Clemson, South Carolina 29634-0973, United States

[‡]Materials Science and Technology Division and [§]Quantum Condensed Matter Division, Oak Ridge National Laboratory, Oak Ridge, Tennessee 37831, United States

Supporting Information

ABSTRACT: A new series of transition metal vanadates, namely, $Ba_2M(VO_4)_2(OH)$ (M = V^{3+}, Mn^{3+}, and Fe^{3+}), was synthesized as large single crystals hydrothermally in 5 M NaOH solution at 580 °C and 1 kbar. This new series of compounds is structurally reminiscent of the brackebuschite mineral type. The structure of $Ba_2V(VO_4)_2(OH)$ is monoclinic in space group $P2_1/m$, a = 7.8783(2) Å, b = 6.1369(1) Å, c = 9.1836(2) Å, β = 113.07(3)°, V = 408.51(2) Å^3. The other structures are similar and consist of one-dimensional trans edge-shared distorted octahedral chains running along the b-axis. The vanadate groups bridge across edges of their tetrahedra. Structural analysis of the $Ba_2Mn(VO_4)_2(OH)$ analogue yielded a new understanding of the Jahn–Teller effect in this structure type. Raman and infrared spectra were investigated to observe the fundamental vanadate and hydroxide vibrational modes. Single-crystal temperature-dependent magnetic studies on $Ba_2V(VO_4)_2(OH)$ reveal a broad feature over a wide temperature range with maximum at ∼100 K indicating that an energy gap could exist between the antiferromagnetic singlet ground state and excited triplet states, making it potentially of interest for quantum magnetism studies.

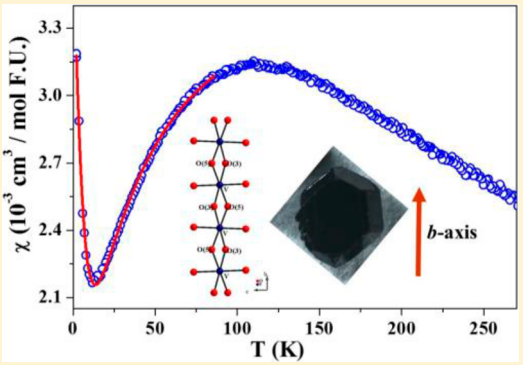

1. INTRODUCTION

The synthesis and characterization of vanadate oxyanion frameworks provide access to materials for a wide variety of applications ranging from batteries[1] to laser optics.[2] Furthermore, multiferroic, magnetic, and other physical properties are also displayed by transition metal vanadate compounds.[3−5] Given the large number of applications of transition metal framework materials, and their complex structure−property correlations, it is essential to investigate the underlying physical phenomena of these compounds. In the case of naturally occurring materials with potentially interesting structure−property relationships but rather complex compositions, it also becomes an important materials chemistry problem to prepare crystals of well-defined stoichiometries to accurately understand these correlations.

We originally began investigating the growth of vanadates as building blocks in optical applications, particularly in their role as laser hosts[6] or luminescent materials.[7−11] The vanadates play a much broader role as a structural building block unit, however. Specifically, they are a member of the class of tetrahedral oxyanions (e.g., PO_4^{3-}, SO_4^{2-}, MoO_4^{2-}) that display extensive structural versatility and can link both d-block and rare earth metal ions in a variety of environments.[12,13] The tetrahedral building blocks can play particularly interesting roles in magnetic solids since they can bridge in multiple environments to generate extended chains, three-dimensional frameworks, or two-dimensional lattices, including those with threefold symmetry leading to spin-frustrated systems with interesting and important magnetic properties.[14]

The tetrahedral building blocks are often more useful as bridging groups than simple oxides or halides in many magnetic studies because the M−O−Td−O−M unit can lead to unusual coupling between the open-shell metal ions. The vanadates have several other unique properties that make them worthy of further study in this regard. They are isoelectronic to the phosphates and can form a huge variety of complexes but with several important differences. In particular the presence of d-orbitals on the central M−O−Td−O−M bridging unit can lead to a variety of unusual coupling effects including reversal of the

Received: May 8, 2015
Published: July 8, 2015

DOI: 10.1021/acs.inorgchem.5b01037
Inorg. Chem. 2015, 54, 7014−7020

Table 1. Crystallographic Data for Compounds 1−4

	1	2	3	4
empirical formula	$Ba_2V(VO_4)_2(OH)$	$Sr_2V(VO_4)_2(OH)$	$Ba_2Mn(VO_4)_2(OH)$	$Ba_2Fe(VO_4)_2(OH)$
FW	572.51	473.07	576.51	577.42
crystal system	monoclinic	monoclinic	monoclinic	monoclinic
crystal dimension, mm	0.34 × 0.22 × 0.18	0.20 × 0.06 × 0.04	0.14 × 0.08 × 0.05	0.24 × 0.12 × 0.05
space group, Z	$P2(1)/m$, 2	$P2(1)/m$, 2	$P2(1)/m$, 2	$P2(1)/m$, 2
T, °C	25	25	25	25
a, Å	7.8783(16)	7.6249(15)	7.8709(16)	7.8750(16)
b, Å	6.1369(12)	6.0903(12)	6.1841(12)	6.1425(12)
c, Å	9.1836(18)	8.8153(18)	9.0589(18)	9.2052(18)
β, deg	113.07(3)	112.15(3)	112.33(3)	113.19(3)
V, Å^3	408.51(2)	379.16(1)	407.88(2)	409.30(2)
2θ range	2.41−25.13	2.49−25.04	2.43−25.04	2.81−25.04
no. of reflections collected	3321	3196	3427	3466
μ (Mo Kα), mm^{-1}	12.824	17.561	13.246	13.429
d_{calc}, g cm^{-3}	4.654	4.144	4.694	4.685
data/restraints/parameters	804/1/83	736/1/82	791/7/83	793/1/83
final R [$I > 2\sigma(I)$] $R1$, $wR2$	0.0231/0.0618	0.0271/0.0704	0.0175/0.0406	0.0177/0.0427
final R (all data) $R1$, $wR2$	0.0234/0.0621	0.0281/0.0752	0.0188/0.0413	0.0180/0.0429
GOF	1.094	1.070	1.006	1.013
largest diff. peak/hole, e/Å^3	1.054/−1.215	0.853/−1.061	0.840/−0.753	0.671/−0.774

classical Goodenough−Kanamori−Anderson superexchange rules,[15,16] and may also lead to so-called supersuper-exchange (SSE).[16] In addition, the coupling constant for tetrahedral oxyanion bridging groups may be reduced to a smaller value than that of typical direct oxo-bridges, so spin frustration may be observed in relatively weak magnetic fields (5−10 T).[17] The vanadate tetrahedra show a considerable tendency to form both one-dimensional chains and two-dimensional layers with interesting long-range magnetic interactions, so they merit particular attention. For example, we recently prepared high-quality single crystals of $K_2Mn_3(VO_4)_2(CO_3)$, which has a honeycomb Mn−O−Mn lattice isolated by VO_4 tetrahedra (*tet*) and also exhibits complex magnetic properties.[18]

From a structural viewpoint the phosphates obviously form an enormous category of solids with an almost unlimited variety of structures with essentially every class of metal ions. A particular source of inspiration in this regard is the class of the various mineral phosphates, wherein a staggering array of beautiful structures with many low-dimensional coordination environments have been reported.[19,20] These can be used as inspiration for what is possible among the XO_4^{3-} (X = P, V) building blocks. The vanadates also have a noteworthy structural library both in the mineralogical[21] and synthetic worlds.[22] The VO_4^{3-} synthons can serve as almost direct analogues to phosphates in many structural variations, but they also adopt a wide range of cluster polyvanadates as well.[23]

Vanadates, of course, also have the additional complication that they can adopt many different oxidation states that lead to significant variations in structural chemistry.[24,25] In addition to leading to structural variations, the lower oxidation vanadates can display a wide range of interesting magnetic properties. An example of the versatility of vanadium oxides is $Ba_8V_7O_{22}$, which actually contains well-ordered examples of three oxidation states of vanadium (V^{3+}, V^{4+}, and V^{5+}).[26] Particular attention has been drawn to low-dimensional vanadium V^{3+} (spin −1) and/or V^{4+} (spin −1/2) chains. For instance, $Ba_2V_3O_9$[27] and $AVGe_2O_6$ (A = Li and Na)[28−30] exhibit rich physical properties due to their rutile-type edge-sharing chains made from VO_6-octahedra (*oct*). At the same time, VO_4^{3-} groups not only assist in the construction of three-dimensional frameworks but also can result in isolated transition metal−oxygen lattices by giving electronically encapsulated magnetic nanostructures.[18]

In this paper we employ high-temperature hydrothermal synthesis to prepare large single crystals of a series of metal vanadate complexes. This enables us to examine the role of vanadate as a low-dimensional bridging building block and try to begin comparing its role to that of phosphate building blocks. We initiate studies of the complex magnetic interactions of the low-dimensional single-crystal solids. In particular we draw inspiration from the massive array of naturally occurring minerals with low-dimensional structures that provide guidance for interpreting new structural types. On the basis of the above motivation, our high-temperature (550−650 °C) hydrothermal crystal growth technique efforts have afforded a new series of transition metal vanadate structures. The $Ba_2M(VO_4)_2(OH)$ (M = V^{3+}, Mn^{3+}, Fe^{3+}) series are derivatives of the brackebuschite-type mineral structure type. Synthesis of well-defined transition metal stoichiometries in the present study has led to a new understanding of the Jahn−Teller effect in this structure type. Additionally, Raman, infrared, and magnetic data are reported for $Ba_2V(VO_4)_2(OH)$.

2. EXPERIMENTAL METHODS

2.1. Hydrothermal Crystal Growth. All hydrothermal reactions were conducted in 2.5 in. long silver ampules with an outer diameter of 1/4 in. Reactants (∼0.2 g total) were loaded with the desired aqueous hydroxide mineralizer solution to fill ∼60% of the remaining volume of the ampule. The silver ampules were welded shut and placed in Tuttle autoclave filled with water to provide suitable counter pressure. The autoclaves were heated to the desired temperature for 6−7 d. After the reaction period, crystals were retrieved from the silver ampules by washing the entire product with deionized water using a suction filtration method. Analytical grade reagents were used as received in all reactions. The chemicals used in this study: BaO (Alfa Aesar, 99.5%), SrO (Alfa Aesar, 99.5%), V_2O_3 (Alfa Aesar, 98%), Mn_2O_3 (Alfa Aesar, 98%), Fe_2O_3 (Alfa Aesar, 98%), and V_2O_5 (Alfa Aesar, 99.6%).

2.2. Synthesis of $Ba_2M(VO_4)_2(OH)$. Crystals of $Ba_2V(VO_4)_2(OH)$ **1** (brown polyhedra) were the first compound isolated in the $Ba_2M(VO_4)_2(OH)$ series using this synthetic technique. BaO (0.0518

DOI: 10.1021/acs.inorgchem.5b01037
Inorg. Chem. 2015, 54, 7014−7020

g), V_2O_3 (0.0253 g), and V_2O_5 (0.1219 g) were loaded into the silver ampules. The reactants were loaded into the silver ampules with 0.4 mL of 5 M NaOH. The welded tubes were heated to 580 °C and kept for 6 d under 1.2 kbar of pressure. Dark brown hexagonal single crystals were isolated as the only product. Larger crystals (2−3 mm) of $Ba_2V(VO_4)_2(OH)$ were synthesized using the same reaction at 650 °C for 10 d. The isostructural $Sr_2V(VO_4)_2OH$ **2** was synthesized from a mixture of SrO (0.0382 g), V_2O_3 (0.0276 g), and V_2O_5 (0.1332 g) in 5 M NaOH mineralizer using similar conditions as the barium analogues. The chemistry of the strontium analogues of Fe^{3+} and Mn^{3+} was attempted under similar conditions but proved to be considerably more complex and is discussed in more detail in the Results Section below. Similarly, $Ba_2Mn(VO_4)_2(OH)$ **3** and $Ba_2Fe(VO_4)_2(OH)$ **4** (brown polyhedra) were also synthesized using similar methods, however, with a lower yield. Pure phases of the Fe and Mn compounds were not observed even at higher temperatures. Other materials, $BaNa_2Fe(VO_4)_2$ and $BaNa_2Mn(VO_4)_2$, were observed as additional products in the iron and manganese reactions, respectively.

2.3. X-ray Diffraction. Single crystals were physically examined and selected under an optical microscope equipped with a polarizing light attachment. The crystals were then mounted on a glass fiber, and data were collected using a Rigaku Mercury CCD detector on an AFC-8S diffractometer equipped with graphite monochromated Mo Kα radiation (λ = 0.710 73 Å). The structure was solved by direct methods using the SHELXTL[31] program and refined on F^2 by least-squares, full-matrix techniques. All non-hydrogen atoms were refined anisotropically. The hydrogen atom of the asymmetric unit was identified from the difference electron density map, and its position was constrained to prevent unreasonable variations in the O−H bond distance. Table 1 reports the crystallographic data of the title compounds, **1**−**4**. Table 2 reports selected bond distances for compounds **1**−**4**. As additional confirmation of the structure refinements, the chemical contents of each compounds were verified by energy dispersive X-ray (EDX) methods and reported in the Supporting Information (Table S1).

Table 2. Selected Interatomic Distances for Compounds 1−4

MO_6	1	2	3	4
M−O(1) × 2	1.999(3) Å	1.983(3) Å	1.930(3) Å	2.008(3) Å
M−O(3) × 2	2.075(3) Å	2.049(3) Å	2.191(3) Å	2.073(3) Å
M−O(5) × 2	2.001(2) Å	2.004(3) Å	1.955(2) Å	2.007(2) Å
$V(1)O_4$				
V(1)−O(1) × 2	1.758(3) Å	1.761(3) Å	1.771(3) Å	1.753(3) Å
V(1)−O(4)	1.671(4) Å	1.658(4) Å	1.658(4) Å	1.673(4) Å
V(1)−O(6)	1.669(4) Å	1.662(4) Å	1.656(5) Å	1.667(4) Å
$V(2)O_4$				
V(2)−O(2) × 2	1.669(4) Å	1.692(3) Å	1.697(3) Å	1.683(3) Å
V(2)−O(3)	1.688(3) Å	1.798(4) Å	1.772(4) Å	1.827(4) Å
V(2)−O(7)	1.669(4) Å	1.668(5) Å	1.681(5) Å	1.670(5) Å

All powder XRD (PXRD) measurements were performed using a Rigaku Ultima IV diffractometer equipped with Cu Kα radiation of λ = 1.5406 Å. PXRD patterns were collected in the range of 5°−65° 2θ with a scan speed of 0.1° min^{-1} with a step size of 0.02° (~10 h scan per sample). PDXL software provided by Rigaku[32] was used for further data analysis.

2.4. Magnetic Measurements. Magnetization measurements were performed using a Quantum Design Magnetic Property Measurement System (MPMS). The data were collected on a 15.2 mg single crystal specimen of $Ba_2V(VO_4)_2(OH)$ oriented such that the crystallographic *b*-axis (the V^{3+} chain direction) is parallel to the applied magnetic field. The temperature-dependent static susceptibility (χ = M/H) measurements were performed on cooling over a temperature range of 300−2 K under an applied magnetic field of 10 kOe. Isothermal magnetization measurements were performed at various temperatures in applied magnetic fields up to 50 kOe.

2.5. Spectroscopic Characterization. Vibrational spectroscopic characterization was performed on ground single crystals of $Ba_2M(VO_4)_2(OH)$. The ground single crystals were mixed and ground together with KBr before pressing into a pellet. The infrared spectrum of the pellet was measured on a Nicolet Magna IR Spectrometer 550 in the frequency range from 400 cm^{-1} to 4000 cm^{-1} with a 4 cm^{-1} resolution. A 514.5 nm wavelength Ar laser (Innova 200, Coherent) was used with 90 mW to obtain the excitation of Raman scattering. Raman scattering was collected using a camera lens of f/1.2 in a 1808 backscattering geometry and analyzed by a triple spectrometer (Triplemate 1877, Spex) equipped with a charge-coupled device (CCD) detector (iDUS 420 series, Andor) cooled to 60 °C. Typical spectrum acquisition time was 10 s. The Raman spectrum of Indine and the Raman spectrum of a 5:2 mixture of chloroform/bromoform was used for spectral calibration. A glass capillary holder was fabricated for suspending the polycrystalline sample of the title compound, in such a way that the plane of the substrate was normal to the collection optics.

3. RESULTS AND DISCUSSION

3.1. Synthesis and Phase Space of the $Ba_2M(VO_4)_2(OH)$ (M = V, Mn, and Fe) Series. The goal of this study was the investigation of new transition metal compounds containing vanadate groups, targeting new low-dimensional bridged structures with potentially interesting structural and magnetic interactions. As with our previous studies, hydrothermal crystal growth proved to be highly effective in preparing large single crystals of novel structures with interesting magnetic and optical properties. Our initial synthetic efforts of the first-row transition metal−vanadate system produced a number of members of the $Ba_2M(VO_4)_2(OH)$ series, where M = V^{3+}, Mn^{3+}, and Fe^{3+}. The $Ba_2V(VO_4)OH$ analogue **1** was first synthesized at 580 °C with 5 M NaOH as the mineralizer. After the initial structure was determined, compound **1** was grown at high temperatures (650 °C) and with longer duration, which proved to increase the size of the crystals to 2−3 mm per edge (Figure 1). Higher mineralizer concentrations of sodium hydroxide (>5 M) did not produce any crystalline vanadate phases. The PXRD pattern for ground

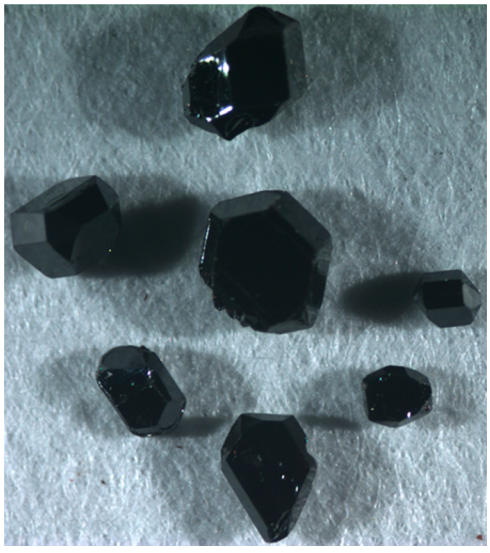

Figure 1. Hydrothermally grown crystals of $Ba_2V(VO_4)_2(OH)$. Crystals are up to 3 mm in size.

DOI: 10.1021/acs.inorgchem.5b01037
Inorg. Chem. 2015, 54, 7014−7020

sample of $Ba_2V(VO_4)_2(OH)$ is shown in Figure 2 versus the calculated pattern, indicating the product was phase-pure.

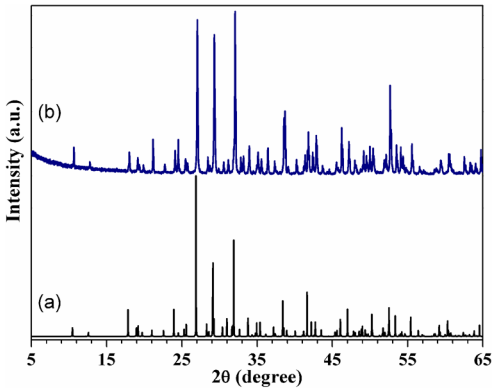

Figure 2. Calculated (a) and experimental (b) PXRD patterns of $Ba_2V(VO_4)_2(OH)$.

Our attempt to grow other trivalent transition metal derivatives such as Mn and Fe was successful leading to formation of single crystals of $Ba_2Mn(VO_4)(OH)$ **3** and $Ba_2Fe(VO_4)(OH)$ **4**, respectively. Unlike the trivalent vanadium analogue, both manganese and iron reactions also produced $Na_2BaMn(VO_4)_2$[33] and $Na_2BaFe(VO_4)_2$ compounds (isostructural with one another), in addition to the target phases **3** and **4**. Such $A_2AEM(VO_4)_2$ phases (A = Na, Ag; AE = Ba, Sr; M = Co, Ni)[3,33] feature a triangular lattice of transition metal again connected via nonmagnetic *tet*-VO_4. These materials were proven to undergo ferromagnetic transitions at lower temperatures. The detailed structures and magnetic behavior of these compounds, including the novel $Na_2BaFe(VO_4)_2$ crystals, will be discussed in an upcoming paper.

This interesting series of $Ba_2M(VO_4)_2(OH)$ compounds motivated us to examine the Sr derivatives of the $Ba_2M(VO_4)_2(OH)$ series as well. However, $Sr_2V(VO_4)_2(OH)$ was the only isostructural derivative that could be synthesized successfully, though still with some impurity phase of SrV_6O_{11}[34] single crystals. The Sr systems did lead to significant new chemistry, and the $SrO-Mn_2O_3-V_2O_5$ system proved to be particularly rich. It produced three different phases, namely, $NaMnVO_4$[35] and the new phases $Na_2SrMn(VO_4)_2$ and $SrMn(VO_4)(OH)$, which will also be the subject of a future paper.

3.2. Crystal Structures of 1−4. Crystallographic data for compounds **1**−**4** are reported in Table 1. This series of compounds crystallize in the monoclinic crystal system with a space group of $P2_1/m$ (No. 11) and possess the brackebuschite−gamagarite type of structure. Despite its interesting structure, limited structural work has been performed on this series in the past because of challenges with crystal quality in naturally occurring specimens. After some preliminary attempts, Foley, Hughes, and Lange were able to reconcile the structures of brackebuschite and gamagarite using a sample of $Pb_2(Mn^{3+},Fe^{3+})(VO_4)_2(OH)$.[36−39] Since then the structures of other minerals with complex compositions such as calderonite and arsentsumebite have also been ascribed to this structure type.[40,41] However, to our knowledge, there has not been thorough investigation or a targeted synthetic approach to crystals of this structure type. In particular, since the crystals display interesting long-range magnetic order, and also the Mn^{3+}-containing system is subject to Jahn−Teller effects, it is especially useful to study the detailed structural properties of pure crystals containing a single transition metal (a situation not presented in the naturally occurring samples).

Here, the structure of **1** will be discussed as the representative example of this family. Figure 3 shows the

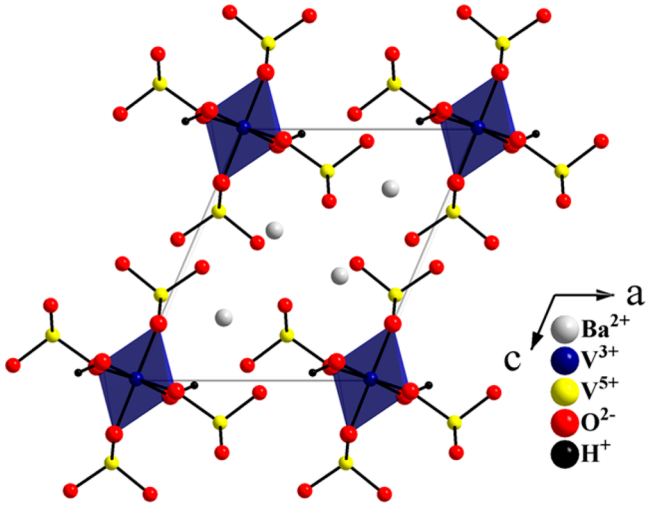

Figure 3. Structure of $Ba_2M(VO_4)_2(OH)$ viewed along [010]. Vanadate-decorated chains of transition metal octahedra are isolated from one another in the *ac* plane, creating the 1-D structure.

basic structural view of $Ba_2V(VO_4)_2OH$ along the *b*-axis. Edge-sharing chains of $[V^{3+}O_6]$ units (*oct*-VO_6) propagate along the *b*-axis, with isolated $[V^{5+}O_4]$ (*tet*-VO_4) branching from each chain. The branched chains are isolated from one another, with Ba^{2+} ions filling the gaps. The structure consists of one unique V^{3+} site and two crystallographically unique V^{5+} sites. Edge-sharing of the *oct*-VO_6 units through O(3) and O(5) form $[VO_4]_\infty$ one-dimensional (1-D) chains along the *b*-axis (Figure 4a). Similar chains have been observed in pyroxene-type structures, including $LiVGe_2O_6$, whose magnetic properties

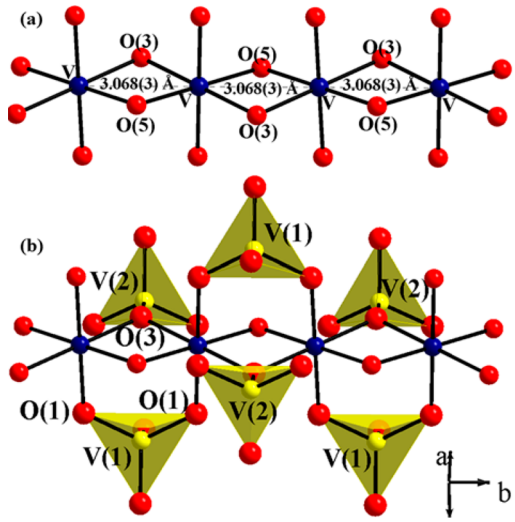

Figure 4. Transition metal chains in $Ba_2M(VO_4)_2(OH)$. Propagation along the *b*-axis occurs via (a) edge-sharing equatorial O(3) and O(5) atoms, and (b) V(1) vanadate tetrahedra chelating axial O(1) atoms. A second vanadate tetrahedron, V(2), binds a single O(3) atom in the chain.

DOI: 10.1021/acs.inorgchem.5b01037
Inorg. Chem. 2015, 54, 7014−7020

were thoroughly investigated.[30] Two *oct*-VO_6 units in the 1-D $[VO_4]_\infty$ chains are further connected by the *tet*-V(1)O_4 unit via the axial oxygen O(1) of each octahedron. At the same time *tet*-V(2)O_4 connects to one of the edge-shared oxygen atoms, O(3), in the $[VO_4]_\infty$ chain (Figure 4b). The other edge-sharing oxygen atom in the $[VO_4]_\infty$ chain, O(5), connects to H featuring the OH^- group in the structure.

From the perspective of interpreting the magnetic properties of the $Ba_2V(VO_4)_2OH$, it is important to pay special attention to the local bond distances and angles with respect to the V^{3+} magnetic centers. Table 2 shows that the V^{3+}−O bond distances in only *oct*-VO_6 range from 1.999(3) to 2.075 (2) Å, comparable to the sum of the Shannon crystal radii[42] (1.990 Å) for a six-coordinate V^{3+} and O^{2-}. Clearly there is only a small distortion of *oct*-VO_6 from its ideal octahedral geometry, where V−O(3) bridging bonds in the $[VO_4]_\infty$ chains are slightly elongated (compare 2.075(3) Å for V^{3+}−O(3) to 2.001(3) Å for V^{3+}−O(5) and 1.999(3) Å for nonbridging V^{3+}−O(1)). This is consistent with a weak 4 + 2 Jahn−Teller distortion for V^{3+} in **1** and **2** and Fe^{3+} in **4**. The resulting V−O−V bridging angles V^{3+}−O(3)−V^{3+} of 95.3(1)° and V^{3+}−O(5)−V^{3+} of 100.1(2)° are observed. As shown in Figure 4a, the V^{3+}−V^{3+} distance in 1-D $[VO_4]_\infty$ chains is 3.068(3) Å. Furthermore, V^{5+}−O bond distances in VO_4 tetrahedra range from 1.669(3) Å to 1.758(3) Å The average V^{5+}−O bond length for *tet*-VO_4 tetrahedra is 1.687(2) Å and is consistent with the ionic radii sum for V^{5+}−O^{2-} 1.685 Å.

The structure of **3** exhibits a much greater degree of distortion about the *oct*-MnO_6 than is observed in structures **1**, **2**, and **4**. This is likely the manifestation of a strong Jahn−Teller effect for Mn^{3+}, which typically produces a significant 4 + 2 type of distortion.[36,43] The degree of the distortion can be quantified by the value Δ, where $\Delta = 1/6\sum[(L_i - \langle L\rangle)/\langle L\rangle]^2$, where L_i and $\langle L\rangle$ are any individual M−O bond distance and the mean M−O bond distance, respectively, for a given MO_6 octahedron. It is interesting to note that the natural sample of brackebuschite contains mixed Mn^{3+} and Fe^{3+} at this site and thus shows a diluted Jahn−Teller effect with Mn/Fe−O bonds of 1.98(2) Å (×2), 1.99(2) Å (×2), and 2.10(2) Å (×2), corresponding to ⟨2.02⟩ and Δ = 0.0007.

The Mn^{3+} octahedra in **3** are not diluted with a weak or inactive Jahn−Teller ion and correspondingly exhibit Mn−O bonds of 1.932(3) Å (×2), 1.955(2) Å (×2), and 2.191(3) Å (×2), with ⟨2.026⟩ and Δ = 0.0033. Such distortion is comparable to other Mn^{3+}-bearing minerals having similar mean Mn−O bond distances such as fredrikssonite,[43] $Mg_2Mn^{3+}(BO_3)O_2$ (⟨2.036⟩, Δ = 0.0025), orientite,[44] $Ca_2Mn^{2+}Mn^{3+}{}_2Si_3O_{10}(OH)_4$ (⟨2.023⟩, Δ = 0.0039), takeuchiite,[45] $(Mg,Mn^{2+})_2(Mn^{3+},Fe^{3+})BO_5$ (⟨2.028⟩, Δ = 0.0042), and the vanadate krettnichite,[46] $(Pb,Sr)Mn_2(VO_4)_2(OH)_2$ (⟨2.037⟩, Δ = 0.0030). The similarity to krettnichite is particularly interesting since that structure features similar chains of edge-sharing octahedra. However, in krettnichite the chains are connected via the vanadate tetrahedra, whereas the vanadate-decorated chains in the title compounds of this study are isolated from one another. The Jahn−Teller distortion is further reflected in the elongated *b*-axis and contracted *c*-axis of **3** compared to the other barium-based species here. In comparison, the other M^{3+} octahedra in **1** (Δ = 0.0003), **2** (Δ = 0.0002), and **4** (Δ = 0.0002) are not distorted to nearly the same degree as the Mn^{3+} octahedra in **3** and are, as expected, less distorted than even the diluted Jahn−Teller distortion in natural brackebuschite, with its random concentrations of Mn^{3+}.

3.3. Preliminary Magnetic Properties of $Ba_2V(VO_4)_2(OH)$. Figure 5 displays the temperature-dependent magnetization of **1**. The susceptibility curve exhibits a broad feature over a wide temperature range with maximum at ∼100 K. Such behavior is a typical signature of low-dimensional magnetism with antiferromagnetic (AFM) correlations in which an energy gap exists between the AFM singlet ground state and lowest excited states. Upon lowering the temperature below ∼10 K, $\chi(T)$ shows an upturn, which is presumably due to the Curie−Weiss contribution of free spins at the ends of finite chains arising from natural crystal defects. The isothermal magnetization measured at 2 K varied linearly with field to the highest measurement field of 50 kOe. No evidence for a long-range magnetic transition is detected down to 2 K, suggesting spin-liquid behavior.[47]

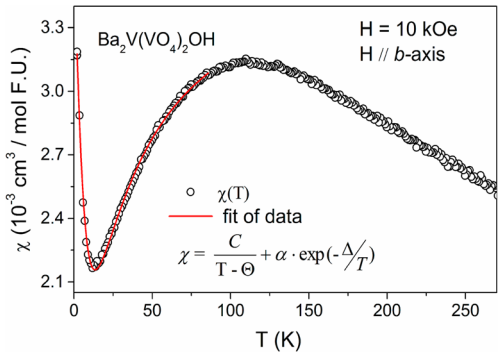

Figure 5. Evolution of the magnetic susceptibility (M/H) as a function of temperature displaying activated behavior characteristic to a spin-liquid state. The red solid line is the fitted curve according to the equation inserted in the figure, yielding an energy gap Δ of 29 K.

To estimate the magnitude of the characteristic energy gap (Δ) between the singlet ground and triplet excited states the low temperature susceptibility data was modeled by the expression: $\chi(T) = C/(T - \Theta) + \alpha \times \exp(-\Delta/T)$, where C is the Curie constant and Θ is the Curie−Weiss temperature. The fit for the temperature range of 2−85 K gives the following values: C = 0.0434 ± 0.0006 cm^3 K/mol, Θ = −11.7 ± 0.2 K, and Δ = 29.0 ± 0.2 K. The magnitude of the Curie constant C indicates that the Curie−Weiss behavior of the susceptibility arises from ∼4% of free spins relative to the total number of V^{3+} ions assuming that S = 1 and g = 2. The activation energy gap is comparable to those found in similar quasi-1-D Haldane chain compounds, $NaV(WO_4)_2$[48] or $SrNi_2V_2O_8$,[49] and classify this material as a potential candidate for studying quantum magnetism.

3.4. Raman and Infrared Spectra of $Ba_2M(VO_4)_2(OH)$. Infrared and Raman spectra for this family of compounds are shown in Figure 6, using $Ba_2V(VO_4)_2(OH)$ as a representative example. For completeness, the infrared and Raman spectra of $Ba_2Fe(VO_4)_2(OH)$ and $Ba_2Mn(VO_4)_2(OH)$, exhibiting qualitatively the same bands, are given in the Supporting Information (Figures S1 and S2). Infrared spectroscopy was used to probe the presence of hydroxide group. Figure 6a shows the infrared spectrum for compound **1**, and the sharp band at 3516 cm^{-1} is, most likely, attributed to the OH^- group found in the unit cell of $Ba_2V(VO_4)_2(OH)$, which is crystallographically constrained as a bridging group between

DOI: 10.1021/acs.inorgchem.5b01037
Inorg. Chem. 2015, 54, 7014−7020

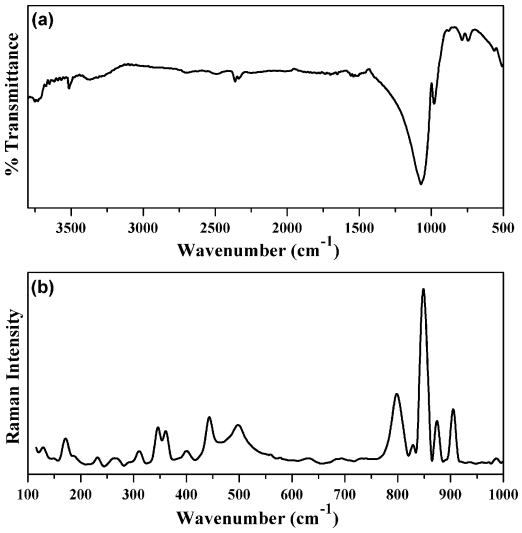

Figure 6. Infrared (a) and Raman (b) spectra of $Ba_2V(VO_4)_2(OH)$.

oct-VO_6 units of the chains. It is noteworthy to mention that the broad infrared band at ~3368 cm^{-1} could be due to the shorter O−H···O bond length of 1.906(4) Å, which could give rise to strong hydrogen bonds in the structure.[50,51] Further, stretching vibrations ν of V−O in *tet*-VO_4 groups occur at 700−1100 cm^{-1}.[51]

The Raman spectrum of $Ba_2V(VO_4)_2(OH)$ displays vanadate scattering in very good agreement with that previously reported for the vesignieite-type struture, $Cu_3Ba(VO_4)_2(OH)_2$, which provides perhaps the best analogue of detailed Raman analysis of this general class of materials.[51] The spectrum of compound **1** in the 100−1000 cm^{-1} region is shown in Figure 6b. The bands in the range of 797−905 cm^{-1} correspond to the symmetric stretching vibrations ν_1 of the $[VO_4]^{3-}$-orthovanadate groups in the structure. The two V−O bands at 848 and 873 cm^{-1} can be taken as an indicator of the presence of two distinct $[VO_4]^{3-}$ groups in the structure. In the region of 100−600 cm^{-1} several symmetric and asymmetric bending modes of $[VO_4]^{3-}$ are observed. The two bands at 497 and 442 cm^{-1} can be assigned to the $[VO_4]^{3-}$ antisymmetric bending modes, and bands at 310, 346, and 361 cm^{-1} can be ascribed to $[VO_4]^{3-}$ symmetric bending modes. The Raman bands below 300 cm^{-1} could be due to the Ba−O or lattice vibrations.

4. SUMMARY AND CONCLUSIONS

Our initial examination of using vanadate building blocks with a high-temperature hydrothermal method is very promising. We succeeded in growing a number of interesting new phases as high-quality single crystals. In particular a series of compounds was obtained having the formula $Ba_2M(VO_4)_2(OH)$, where M = V^{3+}, Mn^{3+}, and Fe^{3+}. All compounds can be grown as high-quality single crystals, but only the V^{3+} material grows phase-pure in our conditions. The chemistry of these systems is very rich, and other reaction combinations form a variety of other interesting materials that will be the subject of a series of future reports. The strontium analogue of V^{3+} also forms cleanly, while Sr versions of Fe and Mn vanadates form a variety of new and unusual compounds under further investigation.

The crystals can be grown in very large sizes (2−3 mm), and this will enable a number of future studies such as single-crystal neutron diffraction. Single-crystal X-ray diffraction demonstrates that the structures are derivatives of the mineral class exemplified by brackebuschite. Structural analysis of the Mn^{3+} analogue has enabled a better understanding of the Jahn−Teller distortion in brackebuschite-type materials. The structure contains linear chains of hexacoordinate M^{3+} ions bridged in three different ways. There is a bridging hydroxy group as well as a μ_2 oxygen atom from a vanadate cis to the bridging hydroxy. Two vanadates also form bridging chelates in the trans position. Other characterization such as Raman and IR spectroscopy supports this analysis. Of these trivalent metal ions the V^{3+} forms the best phase-pure large single crystals and is the subject of future detailed magnetic studies because it is a 1-D chain of S = 1 metal ions. Preliminary magnetic investigation of the V^{3+} analogue does display interesting 1-D magnetic behavior. The present study indicates spin-liquid behavior with potential for quantum magnetic studies.

The structural type discussed herein is a branch of a fairly broad class of minerals with many derivatives including other vanadates as well as alumino phosphates. This demonstrates that the enormous array of minerals constructed of oxyanion building blocks can serve as an intellectual starting point for many new compounds. This is particularly significant because so many of the natural phosphates and vanadates form low-dimensional structures that suggest interesting optical and magnetic properties. Unfortunately native minerals usually make for poor material characterization studies because of low availability or the presence of impurities inherent in nearly all natural minerals. Our ability to prepare pure high-quality single crystals using high-temperature hydrothermal synthesis enables us to perform careful structural, optical, and magnetic studies of these interesting materials and opens up the vast array of interesting mineral structures for further materials property studies.

■ ASSOCIATED CONTENT

Ⓢ Supporting Information

Elemental analysis by EDX for compounds **1**−**4**, infrared and Raman spectra for compounds **3** and **4**, crystal structure data in CIF format. The Supporting Information is available free of charge on the ACS Publications website at DOI: 10.1021/acs.inorgchem.5b01037.

■ AUTHOR INFORMATION

Corresponding Author

*E-mail: kjoseph@clemson.edu.

Notes

The authors declare no competing financial interest.

■ ACKNOWLEDGMENTS

This was work was supported by a grant from the National Science Foundation (DMR-1410727). Work at the Oak Ridge National Laboratory was sponsored by the Materials Sciences and Engineering Division and Scientific User Facilities Division.

■ REFERENCES

(1) Chernova, N. A.; Roppolo, M.; Dillon, A. C.; Whittingham, M. S. *J. Mater. Chem.* **2009**, *19*, 2526−2552.
(2) Fields, R. A.; Birnbaum, M.; Fincher, C. L. *Appl. Phys. Lett.* **1987**, *51*, 1885−1886.
(3) Möller, A.; Amuneke, N. E.; Daniel, P.; Lorenz, B.; Cruz, C. R.; Gooch, M.; Chu, P. C. W. *Phys. Rev. B: Condens. Matter Mater. Phys.* **2012**, *85*, 214422.
(4) Amuneke, N. E.; Tapp, J.; de la Cruz, C.; Möller, A. *Chem. Mater.* **2014**, *26*, 5930−5935.

DOI: 10.1021/acs.inorgchem.5b01037
Inorg. Chem. 2015, 54, 7014−7020

(5) Rogado, N.; Huang, Q.; Lynn, J. W.; Ramirez, A. P.; Huse, D.; Cava, R. J. *Phys. Rev. B: Condens. Matter Mater. Phys.* **2002**, *65*, 144443.
(6) Forbes, A. F.; McMillen, C. D.; Giesber, H. G.; Kolis, J. W. *J. Cryst. Growth* **2008**, *310*, 4472−4476.
(7) Kimani, M. M.; Thompson, L.; Snider, W.; McMillen, C. D.; Kolis, J. W. *Inorg. Chem.* **2012**, *51*, 13271−13280.
(8) Kimani, M. M.; McMillen, C. D.; Kolis, J. W. *Inorg. Chem.* **2012**, *51*, 3588−3596.
(9) Kimani, M. M.; Kolis, J. W. *J. Lumin.* **2014**, *145*, 492−497.
(10) Kimani, M. M.; McMillen, C. D.; Chen, H.; Anker, J.; Kolis, J. W. *J. Solid State Chem.* **2015**, *226*, 312−319.
(11) Kimani, M. M.; McMillen, C. D.; Kolis, J. W. *J. Solid State Chem.* **2015**, *226*, 320−325.
(12) Natarajan, S.; Mandal, S. *Angew. Chem., Int. Ed.* **2008**, *47*, 4798−4828.
(13) Komissarova, L. N.; Zhizhin, M. G.; Filaretov, A. A. *Russ. Chem. Rev.* **2002**, *71*, 619−650.
(14) Ramirez, A. P. *Annu. Rev. Mater. Sci.* **1994**, *24*, 453−480.
(15) Geertsma, W.; Khomskii, D. *Phys. Rev. B: Condens. Matter Mater. Phys.* **1996**, *54*, 3011−3014.
(16) Koo, H.-J.; Whangbo, M.-H. *Inorg. Chem.* **2006**, *45*, 4440−4447.
(17) Bratsch, M.; Tapp, J.; Litvinchuk; Möller, A. *Inorg. Chem.* **2014**, *53*, 4994−5001.
(18) Yakubovich, O. V.; Yakovleva, E. V.; Golovanov, A. N.; Volkov, A. S.; Volkova, O. S.; Zvereva, E. A.; Dimitrova, O. V.; Vasiliev, A. N. *Inorg. Chem.* **2013**, *52*, 1538−1543.
(19) Hawthorne, F. C. *Mineral. Mag.* **1998**, *62*, 141−164.
(20) Hawthorne, F. C. *Acta Crystallogr., Sect. B: Struct. Sci.* **1994**, *B50*, 481−510.
(21) Schindler, M.; Hawthorne, F. C.; Baur, W. H. *Can. Mineral.* **2000**, *38*, 1443−1456.
(22) Zavalij, P. Y.; Whittingham, M. S. *Acta Crystallogr., Sect. B: Struct. Sci.* **1999**, *B55*, 627−663.
(23) Livage, J. *Materials* **2010**, *3*, 4175−4195.
(24) Schindler, M.; Hawthorne, F. C.; Baur, W. H. *Chem. Mater.* **2000**, *12*, 1248−1259.
(25) Borel, M. M.; Leclaire, A.; Chardon, J.; Raveau, B. *J. Mater. Chem.* **1998**, *8*, 693−697.
(26) Liu, G.; Greedan, J. E. *J. Solid State Chem.* **1994**, *108*, 371−380.
(27) Dhaussy, A.-C.; Abraham, F. *J. Solid State Chem.* **1996**, *126*, 328−335.
(28) Emirdag-Eanes, M.; Kolis, J. W. *Mater. Res. Bull.* **2004**, *39*, 1557−1567.
(29) Vasiliev, A. N.; Voloshok, T. N.; Ignatchik, O. L.; Isobe, M.; Ueda, Y. *JETP Lett.* **2002**, *76*, 30−32.
(30) Gavilano, J. L.; Mushkolaj, S.; Ott, H. R.; Millet, P.; Mila, F. *Phys. Rev. Lett.* **2000**, *85*, 409−412.
(31) Sheldrick, G. M. *Acta Crystallogr., Sect. A: Found. Crystallogr.* **2008**, *A64*, 112−122.
(32) Rigaku. *PDXL: Integrated X-ray Powder Diffraction Software*; Rigaku: Tokyo, Japan, 2010.
(33) Nakayama, G.; Hara, S.; Sato, H.; Narumi, Y.; Nojiri, H. *J. Phys.: Condens. Matter* **2013**, *25*, 116003.
(34) Hat, Y.; Kanke, Y.; Kita, E. *Acta Crystallogr., Sect. C: Cryst. Struct. Commun.* **2010**, *C66*, i99−i102.
(35) Ben Yahia, H.; Gaudin, E.; Boulahya, K.; Darriet, J.; Son, W.-J.; Whangbo, M.-H. *Inorg. Chem.* **2010**, *49*, 8578−8582.
(36) Foley, J. A.; Hughes, J. M.; Lange, D. *Can. Mineral.* **1997**, *35*, 1027−1033.
(37) Abraham, K.; Kautz, K.; Tillmanns, E.; Walenta, K. *Neues Jahrb. Mineral., Monatsh.* **1978**, *38*, l93−196.
(38) Basso, R.; Palenzona, A.; Zefiro, L. *Neues Jahrb. Mineral., Monatsh.* **1987**, 295−304.
(39) Donaldson, D. M.; Barnes, W. H. *Am. Mineral.* **1955**, *40*, 597−613.
(40) Zubkova, N. V.; Pushcharovsky, D. Yu.; Giester, G.; Tillmanns, E.; Pekov, I. V.; Kleimenov, D. A. *Mineral. Petrol.* **2002**, *75*, 79−88.
(41) Tango, J. G. D.; La Iglesia, A.; Rius, J.; Santin, S. F. *Am. Mineral.* **2003**, *88*, 1703−1708.
(42) Shannon, R. D. *Acta Crystallogr., Sect. A: Cryst. Phys., Diffr., Theor. Gen. Crystallogr.* **1976**, *A32*, 751−767.
(43) Burns, P. C.; Cooper, M. A.; Hawthorne, F. C. *Can. Mineral.* **1994**, *32*, 397−403.
(44) Moore, P. B.; Shen, J.; Araki, T. *Am. Mineral.* **1985**, *70*, 171−181.
(45) Norrestam, R.; Bovin, J.-O. *Z. Kristallogr.* **1987**, *181*, 135−149.
(46) Brugger, J.; Armbruster, T.; Criddle, A.; Berlepsch, P.; Graeser, S.; Reeves, S. *Eur. J. Mineral.* **2001**, *13*, 145−158.
(47) Mila, F. *Eur. J. Phys.* **2000**, *21*, 499−510.
(48) Bera, A. K.; Lake, B.; Islam, A. T. M. N.; Klemke, B.; Faulhaber, E.; Law, J. M. *Phys. Rev. B: Condens. Matter Mater. Phys.* **2013**, *87*, 224423.
(49) Masuda, T.; Sakaguchi, T.; Uchinokura, K. *J. Phys. Soc. Jpn.* **2002**, *71*, 2637−2639.
(50) Sun, K.; Litvinchuk, A. P.; Tapp, J.; Lorenz, B.; Möller, A. *Inorg. Chem.* **2015**, *54*, 898−904.
(51) Frost, R. L.; Palmer, S. J.; Cejka, J.; Sejkora, J.; Plasil, J.; Bahfenne, S.; Keeffe, E. C. *J. Raman Spectrosc.* **2011**, *42*, 1701−1710.

DOI: 10.1021/acs.inorgchem.5b01037
Inorg. Chem. 2015, 54, 7014−7020